

## THE LIVE PROGRAM: TESTS AND JOINT INTERPRETATION WITHIN SARNET AND ISTC

M. Buck<sup>1</sup>, M. Bürger<sup>1</sup>, A. Miassoedov<sup>2</sup>, X. Gaus-Liu<sup>2</sup>, A. Palagin<sup>2</sup>,  
L. Godin-Jacqmin<sup>3</sup>, C.T. Tran<sup>4</sup>, W.M. Ma<sup>4</sup>, V. Chudanov<sup>5</sup>

CONTRACT SARNET FI6O-CT-2004-509065

- |   |                          |
|---|--------------------------|
| 1) IKE, Stuttgart, Germany              | 4) KTH Stockholm, Sweden |
| 2) Forschungszentrum Karlsruhe, Germany | 5) IBRAE Moscow, Russia  |
| 3) CEA Cadarache, France                |                          |

### SUMMARY

The development of a corium pool in the lower head and its behaviour is still a critical issue. This concerns, in general, the understanding of a severe accident with core melting, its course, major critical phases and timing, and the influence of these processes on the accident progression as well as, in particular, the evaluation of in-vessel melt retention by external vessel flooding as an accident mitigation strategy. Previous studies were especially related to the in-vessel retention question and often just concentrated on the quasi-steady state behaviour of a large molten pool in the lower head, considered as a bounding configuration. However, non-feasibility of the in-vessel retention concept for high power density reactors and uncertainties e.g. due to layering effects even for low or medium power reactors, turns this to be insufficient. Rather, it is essential to consider the whole evolution of the accident, including e.g. formation and growth of the in-core melt pool, characteristics of corium arrival in the lower head, and molten pool behaviour after the debris re-melting. These phenomena have a strong impact on a potential termination of a severe accident. The general objective of the LIVE program at FZK is to study these phenomena resulting from core melting experimentally in large-scale 3D geometry and in supporting separate-effects tests, with emphasis on the transient behaviour.

Up to now, several tests on molten pool behaviour have been performed within the LIVE experimental program with water and with non-eutectic melts ( $\text{KNO}_3\text{-NaNO}_3$ ) as simulant fluids. The results of these experiments, performed in nearly adiabatic and in isothermal conditions, allow a direct comparison with findings obtained earlier in other experimental programs (SIMECO, ACOPO, BALL, etc.) and will be used for the assessment of the correlations derived for the molten pool behaviour. Complementary to other international programs with real corium melts, the results of the LIVE activities also provide data for a better understanding of in-core corium pool behaviour.

The experimental results are being used for the development and validation of mechanistic models for the description of molten pool behaviour. In the present paper, a range of different models is used for post-test calculations and comparative analyses. This includes simplified, but fast running models implemented in the severe accident codes ASTEC and ATHLET-CD. Further, a computational tool developed at KTH (PECM model implemented in Fluent) is applied. These calculations are complemented by analyses with the CFD code CONV (thermal hydraulics of heterogeneous, viscous and heat-generating melts) which was developed at IBRAE (Nuclear Safety Institute of Russian Academy) within the RASPLAV project and was further improved within the ISTC 2936 Project.

### A. INTRODUCTION

During core meltdown accidents in Pressurized Water Reactors (PWR), the behaviour of corium pools in the lower head is still a critical issue. A number of studies have already been performed to pursue the understanding of a severe accident with core melting, its course, major critical phases and timing, and the influence of these processes on the accident progression [1-3]. However, uncertainties in understanding and modelling of these phenomena and their application to reactor scale still persist [4].

For instance, regarding experiments in large scale geometry using water as simulant, COPO II [5] and BALI [6] experiments performed in 2D slice geometry showed clearly higher heat transfer coefficients (20-30%) for the side and bottom boundaries than those in the 3D ACOPO experiments [3], while the upward heat transfer coefficients were only slightly higher. This implies a different top to downward split, which in the reactor case would be important e.g. for the amount of heat transferred to an overlying metallic layer and thus the strength of the focusing effect. Several reasons for the differences have been discussed, mainly related to the presence of a frozen boundary in COPO II and BALI as compared to ACOPO, including importance of an isothermal boundary, surface roughness of the crust or non-linearity in fluid properties due to large temperature differences between pool and boundary. Clear conclusion could not yet be drawn.

Another yet unresolved question is related to the existence of mushy layers or sharp interfacial boundaries along crust boundaries in the case of non-eutectic melt. Different approaches exist, either assuming a mushy layer with larger temperature differences between melt bulk and pool boundary, but smaller heat transfer coefficients due to increased viscosity caused by solid fractions, or sharp liquid/solid boundaries with the surface temperature at liquidus temperature, thus smaller temperature differences but larger heat transfer coefficients. The experimental and theoretical studies performed up to now did not yield a decision yet.

In order to address these questions and to complement the experimental data on melt pool behaviour in the vessel lower head, FZK performs large-scale tests through the LIVE program [7]. The LIVE tests are designed to investigate the core melt behaviour in the lower plenum of the reactor pressure vessel and the influence of the cooling of the vessel outer surface with water in the conditions that may occur during core meltdown accident in PWRs. To simulate the corium melt a non-eutectic binary mixture of  $\text{NaNO}_3$  and  $\text{KNO}_3$  is used.

The information obtained from the LIVE experiments includes the melt temperature evolution during different stages of the test, the heat flux distribution along the reactor pressure vessel wall in transient and steady state conditions, the crust growth velocity and the influence of the crust formation on the heat flux distribution along the vessel wall. In the post-test analysis crust thickness profile along the vessel wall, the crust composition and the morphology are determined. The experimental results are being used for the development of mechanistic models for the description of in-core molten pool behaviour and their implementation in severe accident codes.

Within the frame of the network of excellence SARNET of the EU 6<sup>th</sup> Framework Program [9], joint post-test calculations and evaluations using different model approaches and codes were performed. The code applications aimed at assessing the capabilities of the existing modelling and identifying possible need for improvements as well as providing support for the interpretation of the experimental results. For the present paper, mainly the experiment LIVE-L1 was the subject of the comparisons.

In the following sections, the experimental facility and procedure are briefly described and main results of the experiment LIVE-L1 are given. Then, the results of the different code applications are presented and discussed.

## **B. EXPERIMENTAL SET-UP**

The main part of the LIVE test facility is a 1:5 scaled Reactor Pressure Vessel of a typical pressurized water reactor (Figure 1). The inner diameter of the test vessel is 1 m and the wall thickness is 25 mm. The material of the test vessel is stainless steel.

To investigate both the transient and the steady state behaviour of the simulated corium melt, an extensive instrumentation of the test vessel is realized. The vessel wall can be equipped with up to 17 instrumented plugs at different positions along 4 meridians at  $0^\circ$ ,  $90^\circ$ ,  $180^\circ$  and  $270^\circ$ . Each plug consists of a heat flux sensor and 5 thermocouples. The thermocouples are protruding into the melt with different distances from the vessel wall (0, 5, 10, 15, 20 mm). The heat flux sensor is a part of the vessel wall and is positioned 1 mm below the inner surface of the test vessel. This sensor measures the heat flux and the corresponding temperature. To measure the temperature at the outer surface of the vessel wall, 17 thermocouples are located at different positions along the four meridians. In addition to the 85 thermocouples of the plugs, it is possible to place up to 80 thermocouples in the melt to measure the temperatures of melt and the crust growth.

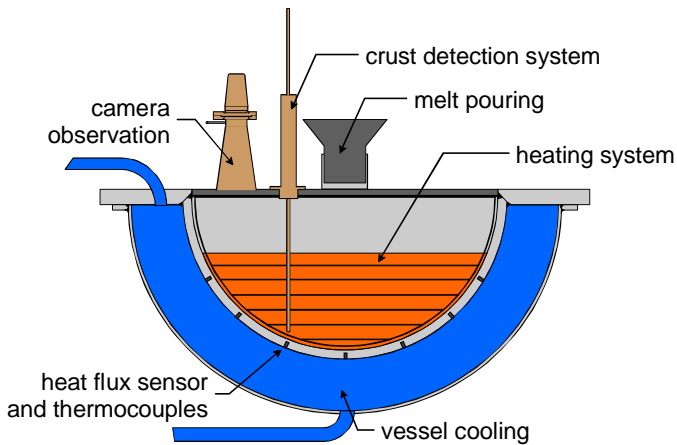


Figure 1. LIVE test vessel.

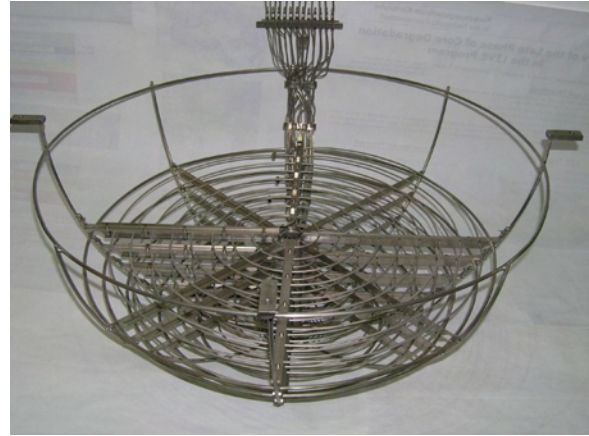


Figure 2. LIVE volumetric heating system.

Decay power input into the melt is recorded and melt samples are extracted during the tests. Different openings in the upper lid of the test vessel allow pouring of the melt to the central region or close to the perimeter of the lower head. To be able to investigate the crust, which is formed at the wall of the vessel, the residual melt is extracted from the vessel at the end of the test to uncover the crust.

To investigate the influence of different external cooling conditions on the melt pool behaviour, the test vessel is enclosed by a second vessel (cooling vessel) to be able to cool the test vessel at the outside. The cooling water inlet is located at the bottom of the cooling vessel and the outlet is positioned at the top of the vessel.

The volumetric heating system has to simulate the decay heat released from the corium melt. Consequently, the heating system has to produce the heat in the melt as homogeneously as possible. Therefore a heater grid with several independent heating elements was constructed (Figure 2). The heating elements are shrouded electrical resistance wires. The maximum temperature the heating system can provide is limited to 1100 °C. To allow the homogeneous heating of the melt pool, the heating system has six heating planes at different elevations with a distance of about 45 mm. Each heating plane consists of a spirally formed heating element with a distance of ~40 mm between each winding. The heating elements are located in a special cage to ensure the correct positioning. All heating planes together provide a maximum power of about 28 kW. Each plane can be controlled separately to allow the homogeneous heat release in the melt.

### C. MAIN RESULTS OF THE LIVE-L1 EXPERIMENT

The experiment LIVE-L1 was dedicated to investigate the core melt behaviour in the lower plenum of the reactor pressure vessel and the influence of the cooling of the vessel outer surface with water in the conditions that may occur during core meltdown accident in the WWER-1000 plant. The test was prepared and performed in the frame of the LACOMERA Project [12] of the EU 5<sup>th</sup> Framework Program jointly with the Technical University of Sofia, Bulgaria. Test initial conditions and main parameters are summarized in Table 1.

To simulate the corium melt a binary mixture of 20 mole% of sodium nitrate  $\text{NaNO}_3$  and 80 mole% of potassium nitrate  $\text{KNO}_3$  with liquidus temperature of ~300 °C and solidification range of about 60 K has been used (Figure 3). The mixture has been melted in the separate heating furnace and when the temperature reached ~350 °C, 120 l of the melt has been centrally poured into the

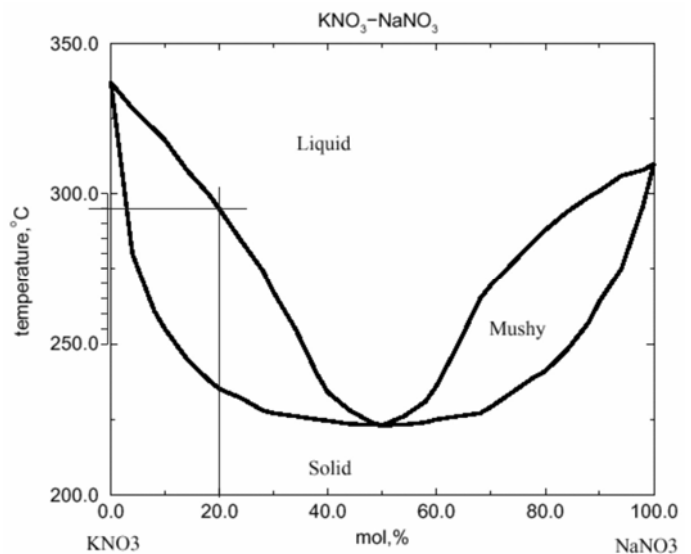


Figure 3.  $\text{KNO}_3$ - $\text{NaNO}_3$  phase diagram.

LIVE test vessel through the pouring spout preheated up to  $\sim 350$  °C. Maximum pouring rate was  $\sim 7$  kg/s.

After the completion of the pouring process a total heating power of approximately 18 kW was applied to homogeneously heat the melt by switching all six heating planes simultaneously. The heating power distribution between the planes is shown in Figure 4.

The melt temperatures measured inside the melt pool indicated that directly after the melt pour the pool temperature decreased to  $\sim 300$  °C at the bottom of the test vessel and to  $\sim 330$  °C near the melt surface. After the start of heating the maximum melt temperatures started to increase. To avoid the overheating of the melt the power was stepwise reduce to  $\sim 10$  kW within 3720 s and was kept at this level. The distortions at the levels 1 and 2 located at the upper part of the melt pool are due to the automatic switch-off of the power when the heater temperatures exceed 380 °C in order to protect the melt from the overheating and decomposition. During this time the maximum melt temperatures increased up to  $\sim 370$  °C (Figure 5).

Flooding of the vessel outer wall was started at 7220 s first with 1.5 kg/s to fill the gap between the cooling vessel and the test vessel wall and then with  $\sim 47$  g/s. This flow rate has been kept constant throughout the whole experiment. Water temperature at the inlet amounted to  $\sim 10$  °C.

After the cooling initiation the maximum melt temperatures at the upper part of the melt pool decreased to  $\sim 320$  °C (Figure 5). At the inner surface of the vessel wall the crust started to form and continued to grow.

The homogeneous heating of the melt with  $\sim 10$  kW was continued for about 20 hours to reach the steady state conditions. Afterwards the heating power was reduced to 7 kW to observe the influence of the power reduction on the crust growth and heat flux distribution and kept at this level for another 6 hours. During this phase the maximum melt temperature decreased to  $\sim 300$  °C.

In the LIVE-L1 test, the heat fluxes through the vessel wall in the transient and steady-state phases were measured along one half-meridian of the vessel. The results of heat flux measurements are presented in

**Table 1. Main parameters and test phases of the LIVE-L1 test**

<b>Melt Characteristics</b>	Type	NaNO <sub>3</sub>	KNO <sub>3</sub>
	Mole %	20%	80%
	Mass %	17.37%	82.63%
	Mass	58 kg	278 kg
	Melt pour	120 l (corresponds to $\sim 31$ cm melt height)	
	Initial temperature	350 °C	
<b>Melt pour</b>	Position	central	
	Number of pours	1	
	Furnace tilting velocity	0.5°/s	
	Furnace target angle	80°	
	Hold time	50 s	
	Pouring spout temperature	350 °C	
<b>Phase 1. Homogeneous heat generation (0-82675 s)</b>	Boundary conditions	Air	
	Heating planes	All	
	Heating power	18 kW at the beginning, reduced to 10 kW at 3720 s	
	Maximum melt temperature	350 °C	
<b>Phase 2. Start of the vessel outer wall cooling (7220 s)</b>	Boundary conditions	water, continuous cooling	
	Cooling water flow rate	Starting with 1.5 kg/s then reduced to $\sim 47$ g/s	
	Heating planes	all	
	Heating power	10 kW	
	Heat generation	homogeneous	
<b>Phase 3. Reduction of heat generation (82675 s)</b>	Boundary conditions	water, continuous cooling	
	Cooling water flow rate	$\sim 47$ g/s	
	Heating planes	all	
	Heating power	7 kW	
	Heat generation	homogeneous	
<b>Phase 4. Test termination, melt extraction (102620 s)</b>	Test conditions	Reaching of the steady-state conditions in Phase 3	
	Heating power	0 kW	

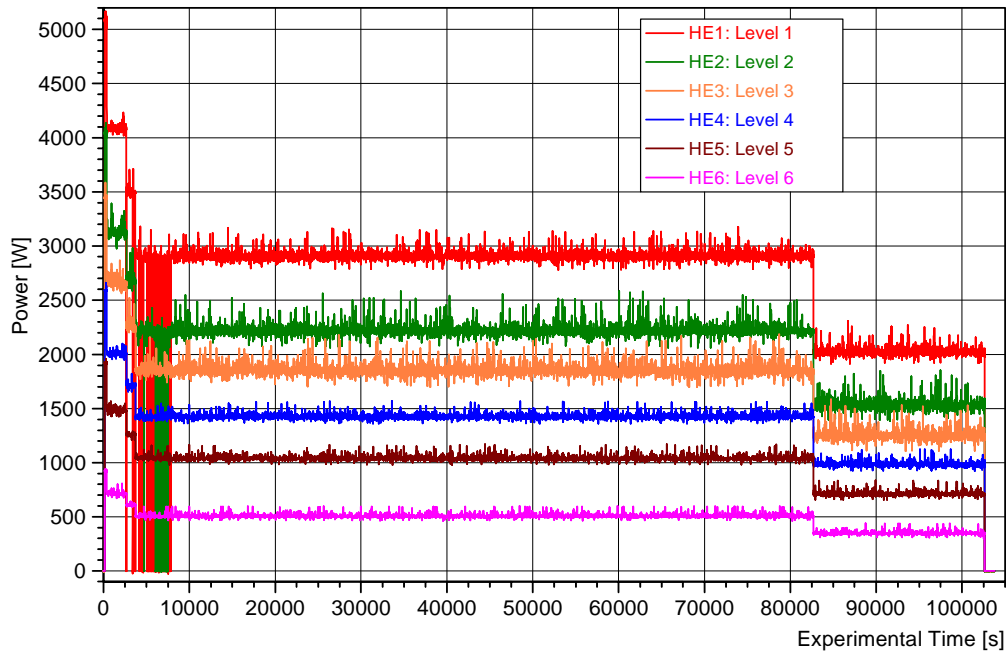


Figure 4. Heating power distribution between the six heating planes in the LIVE-L1 test.

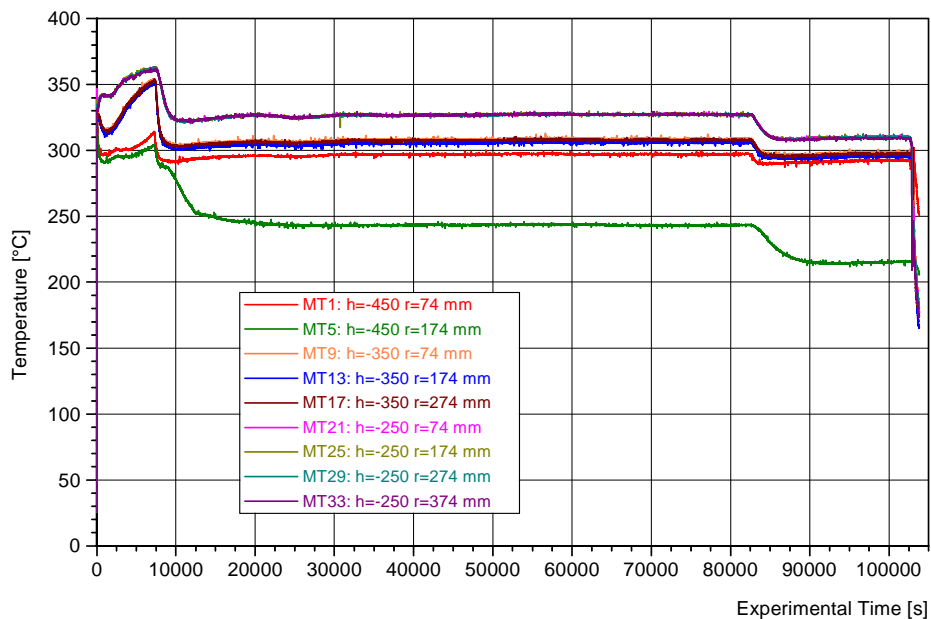


Figure 5. Melt pool temperatures measured at different elevations.

Figure 6 (left). The measurements clearly show two peaks: one after the melt pouring and another one after the start of the vessel outer wall cooling. The maximum heat flux of  $\sim 170 \text{ kW/m}^2$  was measured during the vessel cooling at  $51^\circ$  (approximately at the middle of the melt pool). In the steady-state phase the value of the maximum heat flux through the vessel wall has been decreased to  $\sim 15 \text{ kW/m}^2$ , as detected at  $65.5^\circ$  location (near to the melt surface). Angle  $0^\circ$  corresponds to the south pole of the test vessel.

From the heat flux measurements the fraction of heat extracted through the side wall has been estimated. According to Figure 6 (right), about 80% of the heat generated in the pool is removed through the vessel wall. The remaining part of the heat is removed through the top surface of the pool by radiation and convection to air.

The experiment was completed by switching off the volumetric heating and by the extraction of the liquid melt back into the heating furnace to uncover the crust formed during the test. The measurements of

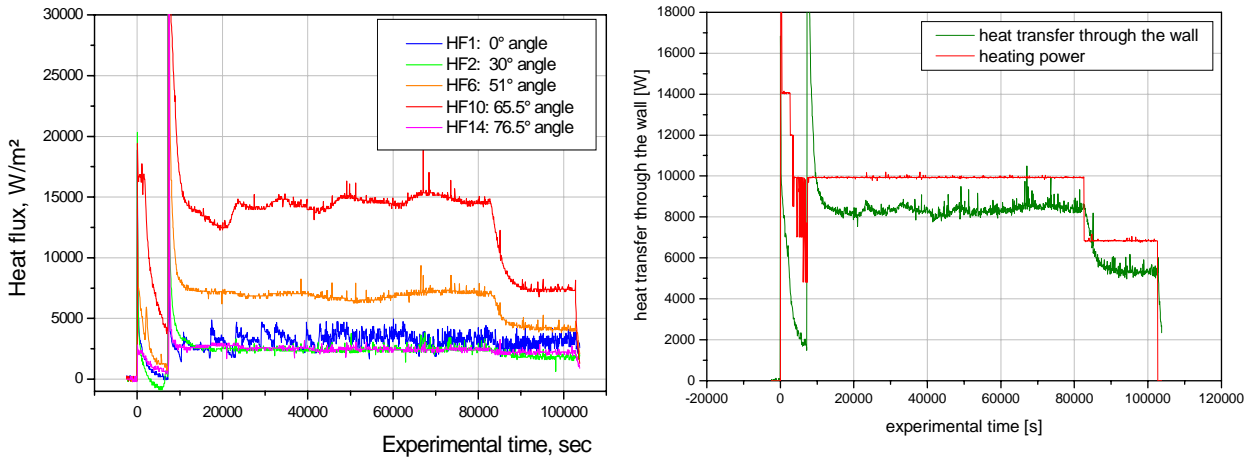


Figure 6. Heat fluxes measured at different positions (left) and power balance (right) in the LIVE-L1 test.

the crust thickness along the vessel wall are presented in Figure 7. They show that the crust thickness varies between  $\sim 11.7$  mm at the position near to the melt surface and  $\sim 70.7$  mm at the bottom of the test vessel.

During the test two melt samples have been extracted from the melt pool, one at the beginning of the test and another one at the end just before the melt extraction from the test vessel. The analysis of the samples is important in two aspects: 1) comparison of the real melt composition with the composition planned for the test, and 2) evaluation of the changes in the melt composition caused by the crust formation and depletion of the high temperature melt component  $\text{KNO}_3$ .

The results of the chemical analysis of the extracted melt samples clearly demonstrate that the real melt composition was very close to the planned one and that the initial  $\text{KNO}_3$  fraction was reduced by  $\sim 1.6$  mole-% at the end of the experiment. This observation is in a good agreement with the post-test chemical analysis of the crust performed at two locations (Table 2), which indicated that the amount of  $\text{KNO}_3$  in the crust has been increased to  $\sim 91$  mole-% compared to initial value of 80 mole-%.

For the interpretation of the results on crust thickness it is important to know the heat conductivity of the crust. The temperature measurements from the crust thermocouples trees have been used to calculate the heat conductivity (assuming constant local heat fluxes during the steady-state periods). Values between 0.37 and 0.66 W/(m K) were obtained, with the majority of the values between 0.45 and 0.5 W/(m K). This is close to the heat conductivity of the melt around the liquidus temperature, which is about 0.46 W/(m K). The spread in the local values of the heat conductivities can be explained by local differences of the porosity of the crust. Such differences have been observed in the post-test examination and are assumed to originate from different local cooling rates during the formation of the crust.

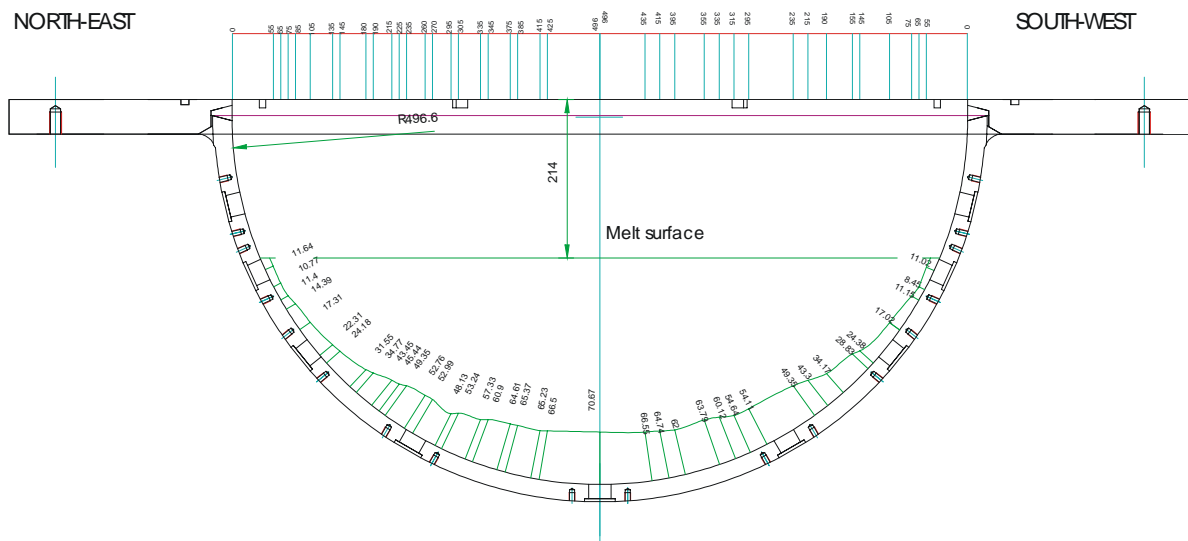


Figure 7. Crust thickness profile at the end of the LIVE-L1 test.

**Table 2. Comparison of the crust and melt composition measured in LIVE-L1 experiment**

	Before the test (sample L1-M1)	After the test (sample L1-M2)	Crust (sample L1-C1)	Crust (sample L1-C2)
K, w%	30.6	28.1	38.9	38.0
Na, w%	4.5	4.6	2.1	2.1
Na/K ratio, w/w	0.15	0.16	0.05	0.06
K, mole %	79.9	78.3	91.5	91.3
Na, mole %	20.1	21.7	8.5	8.7
Na/K ratio, mol/mol	0.25	0.28	0.09	0.095
KNO <sub>3</sub> , w%	82.6	81.1	92.8	92.6
NaNO <sub>3</sub> , w%	17.4	18.9	7.2	7.4

## D JOINT INTERPRETATION OF LIVE EXPERIMENTS

The experimental results of the LIVE programme are being used for the development and validation of mechanistic models for the description of molten pool behaviour. In the present paper, the LIVE test L1 was selected to compare the results of models with different degree of detail, including the simplified, but fast running models implemented in the severe accident codes ASTEC and ATHLET-CD and the PECM model, which can be used for 2D/3D analysis.

These calculations are complemented by analyses with the CONV code (thermal hydraulics of heterogeneous, viscous and heat-generating melts), which was applied to the test LIVE-FSt4, an experiment carried out with water as melt simulant. These calculations give a perspective to future, more detailed simulations with CFD tools.

### D.1 APPLICATION OF THE DIVA MODULE OF THE ASTEC V1.3 CODE TO THE LIVE-L1 EXPERIMENT

The analysis of the LIVE-L1 experiment was performed in the frame of the SARNET Project of the EU 6<sup>th</sup> Framework Program at CEA with the ASTEC code [13]. The ASTEC integral code is being jointly developed by IRSN and GRS to describe the behaviour of a whole severe accident sequence in Light Water Reactors, including the behaviour of engineered safety systems and procedures used in severe accident management. The ASTEC code has a modular structure, each of its modules simulating a reactor zone or a set of physical phenomena. Thus, the ASTEC V1.3 version [10] was used for the analysis of the LIVE-L1 experiment, namely the module DIVA responsible for the in-vessel degradation phenomena. In the near future the CESAR module will be used for the ex-vessel cooling phenomena. In the first step, the module DIVA was utilized with imposed boundary conditions for the external cooling of the vessel.

In the ASTEC V1.3 integral code, the DIVA module is used to describe in-vessel core degradation, core thermal hydraulics and molten pool behaviour in the lower head during severe accident. This stand-alone module was applied for the analysis of the molten pool behaviour in the LIVE-L1 experiment. The external cooling of the vessel outer wall surface was simulated using boundary conditions for the temperature and the heat transfer coefficients at different positions of the vessel wall derived from the test measurements. The following results were obtained from the DIVA calculation and compared with the experimental data:

- temperatures of the inner and outer wall surface,
- temperature distribution in the molten pool,
- crust thickness.

The DIVA input deck was developed at CEA, the geometrical characteristics of the test facility and the physical properties of the 20-80 mole% NaNO<sub>3</sub>-KNO<sub>3</sub> binary melt were taken from [8] and [14]. The external heat exchange coefficients were calculated based on experimental measurements of the heat fluxes,

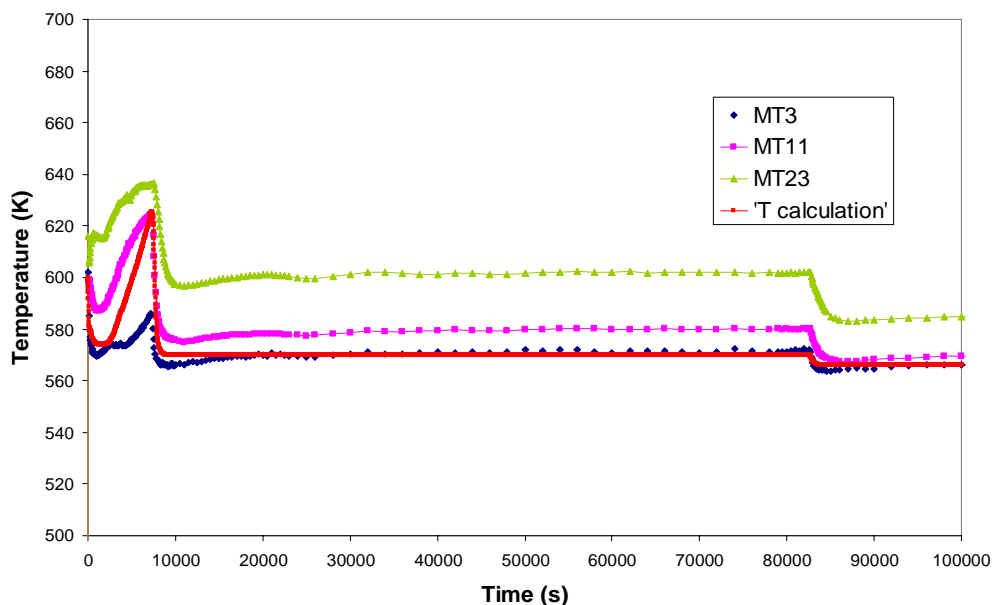


Figure 8. Melt temperature comparison.

outer wall temperatures and temperatures of the cooling tank. All the experimental phases (see Table 1) were included into the DIVA input deck.

The ASTEC lower plenum model does not allow the treatment of one homogeneous oxide layer in several sub-layers. The molten pool in the LIVE-L1 test was therefore treated as a single layer in the DIVA calculation, with only one representative (average) temperature for the melt in the pool. The sum of the power generated by all six heating planes was homogeneously distributed in this layer. Due to the modelling, it was not possible to reproduce the temperature distribution in the pool (Figure 5) since the code calculates the “effective” temperature of the single layer. This temperature evolution is compared in Figure 8 with the central pool measurements from bottom to top MT3, MT11 and MT23. Globally, the experimental trend is obtained even if the calculated temperature is 10 K to 20 K lower than the measured temperatures after the start of the external cooling of the vessel wall.

Inner and outer vessel wall temperatures also show discrepancy during the water cooling and crust formation as shown in Figure 9 and Figure 10. Figure 9 gives the inner vessel wall temperature comparison: from the bottom going up along the wall, the calculated variables T-mesh61, T-mesh64, T-mesh 68 and T-mesh 71 are respectively compared to the thermocouple measurements IT1, IT3, IT7 and IT11. Figure 10 shows the outer vessel wall temperature comparison: again, from the bottom going up along the wall, the calculated variables T-mesh1, T-mesh5, T-mesh 9 and T-mesh 11 are respectively compared to OT1, OT5, OT9 and OT13. In both cases, the calculated temperatures at their maximum are about 40 K higher than the experimental values.

From the validation point of view it seems important to compare the ASTEC/DIVA calculations of the crust thickness between the corium layer and the vessel wall. Unfortunately, the crust thickness is not directly provided as a standard output of DIVA. To calculate the crust thickness, an approach has been implemented based on the assumptions of steady-state conditions and a linear temperature gradient through the crust as, done in DIVA [15]. Setting the heat flux from the pool towards the crust equal to the heat flux through crust and vessel wall, the crust thickness can be calculated using known values from the calculation for the melt pool temperature, the melting temperature of the pool mixture, the heat local transfer coefficient between the melt pool and the crust, the outer temperature of the vessel wall, the thickness and heat conductivity of the vessel wall as well as the heat conductivity of the crust. The calculation procedure is described in more detail in [16].

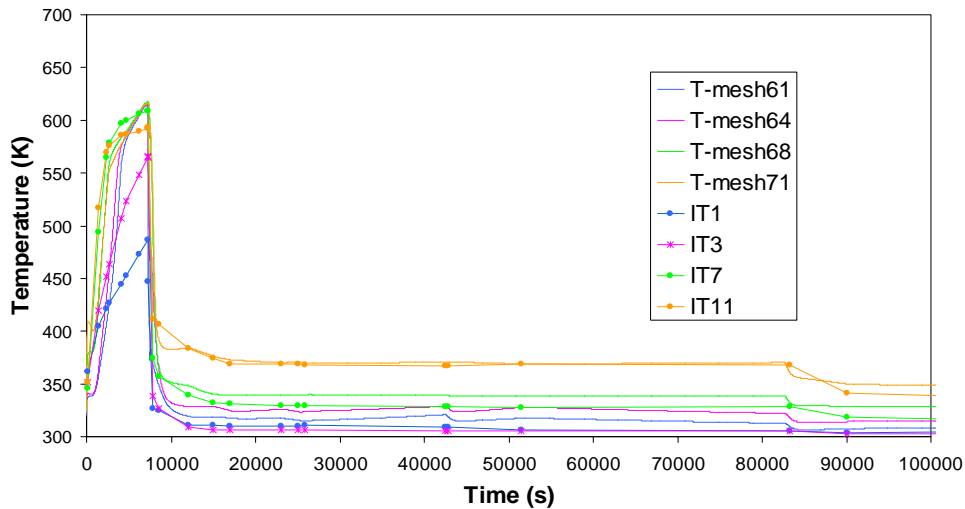


Figure 9. Temperatures of the inner vessel wall calculated by the DIVA module.

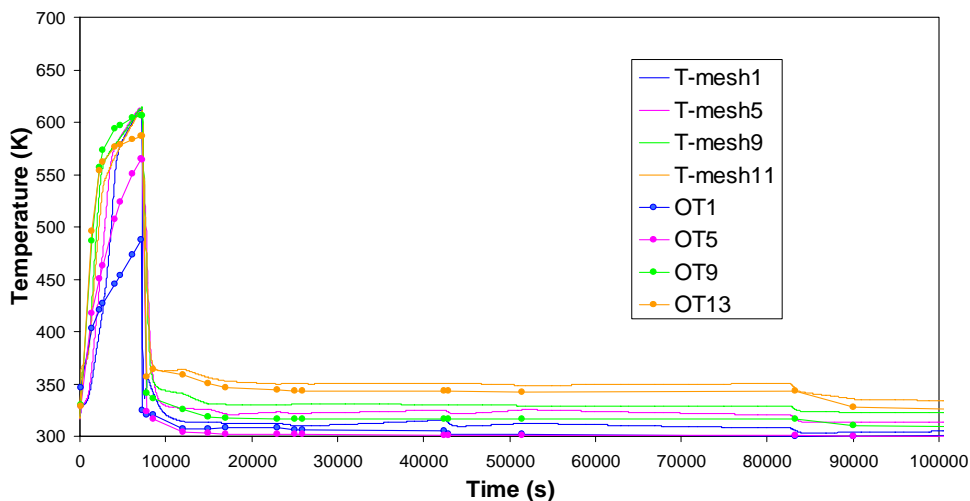


Figure 10. Temperatures of the vessel outer wall calculated by the DIVA module.

The value of the thermal conductivity of the crust is subject to some uncertainty (see Section C). A sensitivity study was performed to evaluate the influence of different values of the thermal conductivity on the final crust thickness. Further, the effect of a delay between power shut-down (at 102629 s) and melt extraction was checked. The results are shown in Figure 11. According to this, best agreement with the experimental crust thickness is obtained assuming a conductivity of 0.68 W/(m K) or a lower conductivity of 0.54 W/(m K) and a delay of 100 s between shut-down and extraction.

For these cases, keeping also in mind the simplified approach (e.g. steady-state conditions, use of single melting temperature for a non-eutectic melts), the calculated crust thickness profile corresponds well to the experimental values determined post-test except for the radius locations between 0.24 m and 0.28 m. This approach is, however, not applicable to the calculations of the crust thickness evolution in the transient phases of the experiment due to the limitations described above.

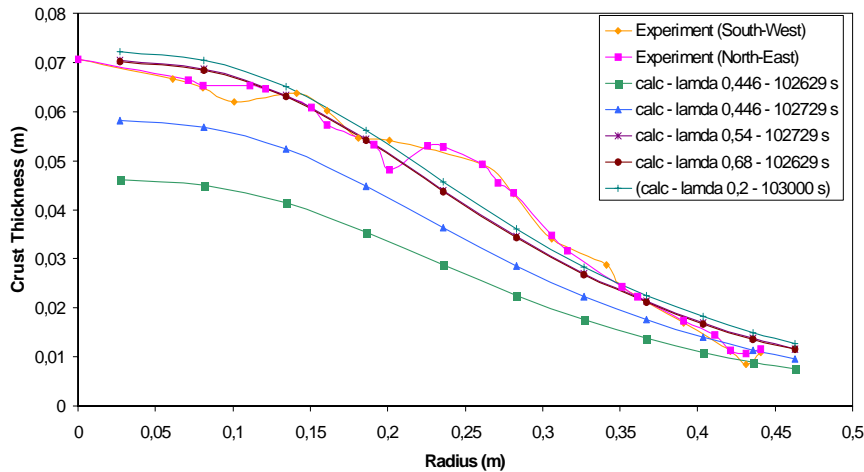


Figure 11. Crust thickness profile calculated by the DIVA code

## D.2 CALCULATIONS USING THE MELT POOL MODEL OF ATHLET-CD LATE-PHASE MODULES

The MEWA and VECO modules are being developed and integrated in the German system code ATHLET-CD [18] for the description of late phase core melting. MEWA describes the processes of late phase core degradation with massive melting, melt relocation, molten pool formation and behaviour up to the relocation of melt to the lower head. The VECO module is designed to model the behaviour of corium in the lower head, including debris formation, coolability, debris re-melting and molten pool behaviour up to failure of the RPV.

MEWA and VECO are generally based on a quasi-continuum approach. However, for the description of molten pools, both in the core and in the lower head, an approach based on a representative model is applied. The pool modelling follows the ideas of the FLUXBAIN model [19]. The underlying conceptual picture divides the pool into a boundary layer along the cooled wall where the melt flows down, a stratified lower region in the central lower part of the pool and a turbulent, isothermal region in the upper part. For the heat transfer in the boundary layer, the model of Chawla and Chan [20] is used. The temperature distribution in the central part of the pool is determined from a one-dimensional energy conservation equation in axial direction, assuming that mass flowing down in the boundary layer is balanced by a corresponding upward mass flow in the central pool part. Heat transfer to the surface of the upper mixed layer is described by empirical correlations.

The development of crusts (at side or top) is modelled through a time-dependent mass conservation equation for the layer thickness, assuming a steady-state parabolic temperature profile in the crust, which allows to consider also volumetric heating in the crust. If a crust exists, the interfacial temperature with the molten pool is assumed to be the liquidus temperature, corresponding to the melt composition. The representative pool/crust model is thermally coupled to its environment, e.g. a surrounding debris bed or the vessel wall. More details of the model are given in [21].

Calculations were performed with the melt pool model in MEWA respectively VECO in stand-alone mode. The vessel wall was described as a two-dimensional heat conducting structure. As boundary conditions at the outer vessel surface, the temperature of the cooling water and a heat transfer coefficient (derived from experimental measurements of heat flux and outer cooling tank temperatures) was applied. At the pool surface, radiation towards the uncovered vessel and to the surrounding was modelled.

The pool modelling in MEWA and VECO includes the option to apply a simplified description using a uniform melt temperature in the pool and empirical correlations for the heat transfer to the top and side pool boundaries. Correlations for 3D hemispherical geometry, including angular dependence of the heat flux, are available from [3] and [22], derived from ACOPO and BALI experiments, respectively. Through comparison with these correlations, also the actual LIVE tests can be related to the underlying experiments.

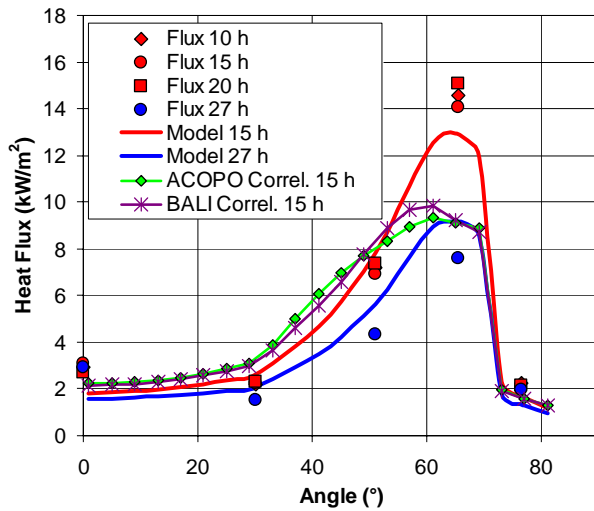


Figure 12. Outer vessel heat flux during steady states calculated by the MEWA module.

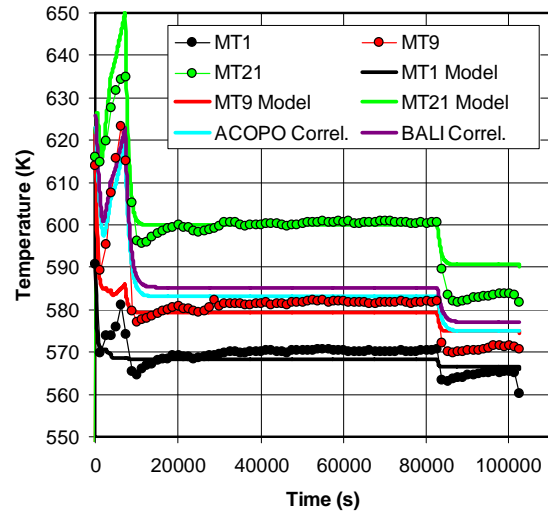


Figure 13. Development of melt temperatures in the pool centre. MT1 is at 50 mm, MT9 at 150 mm and MT21 at 250 mm distance from bottom.

Figure 12 gives a comparison of measured and calculated heat fluxes for the steady state periods with 10 kW (between 10 and 20 h) and 7 kW (after 27 hours) calculated correlations. For the BALI and ACOPO correlations only the high power case is included. It can be seen that using the correlations, the heat flux towards the vessel wall is generally underestimated. This is explained by the fact that the correlations were derived for a cooled upper boundary (crust). In the calculation, for the LIVE-L1 experiment without active top cooling they predict a top to sideways partitioning of the heat flux of about 35/65. Experimentally, rather a partitioning of 20/80 results (see Figure 6).

In the calculation with the full pool model the correlation for the top heat flux was adapted to yield the experimental split. With this modification, the calculated heat flux distribution agrees well with the measurements. It has to be noted that an adaptation of the BALI and ACOPO correlations to the experimental power split would still have resulted in a much too flat power distribution. The peak at 65° can only be recovered by taking into account the temperature distribution in the melt pool (see Figure 13). During the 10 kW heating period, the measured melt temperatures are well met by the calculation. In the 7 kW period the melt temperatures are generally over-estimated. Considering that the calculation rather predicts larger heat fluxes, this means that the sideways heat transfer coefficients are under-estimated for the low power.

Calculated and measured inner and outer vessel temperatures are given in Figure 14. The good

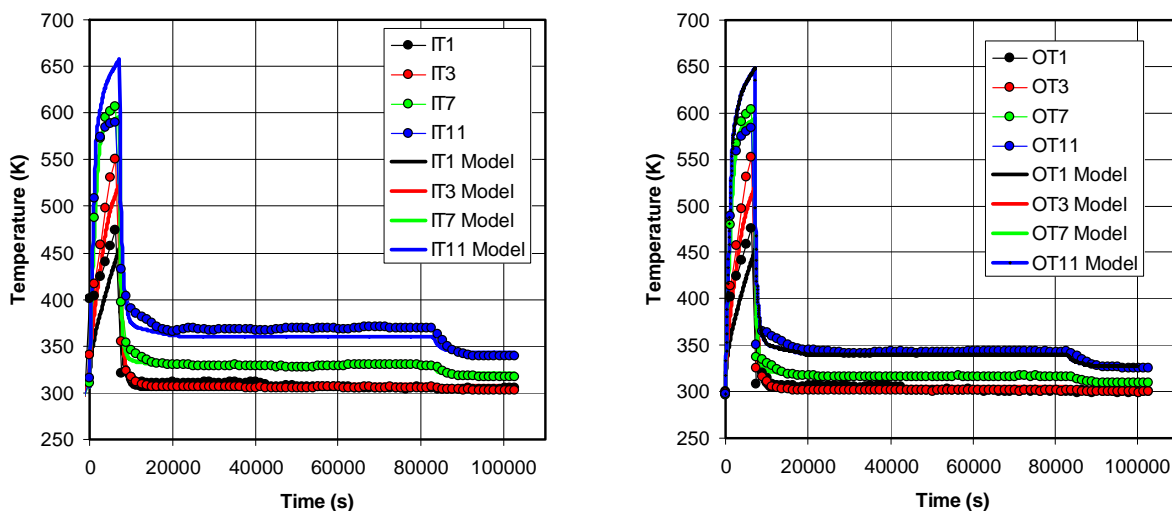


Figure 14. Temperatures at the inner (left) and outer (right) vessel boundary calculated by the MEWA module.

agreement for the steady-state periods is consistent with the heat flux distribution. For the transient period up to start of the water cooling there are however larger discrepancies, also concerning the melt temperatures. These can partly be explained by uncertainties concerning boundary conditions associated with the air cooling. Also, the prediction is complicated by temporal growth and disappearance of crust.

Looking at the experimental heat flux distribution, a higher value at the pole than at 30° can be observed. From a picture of the broken crust taken after the experiment (Figure 15) it can be seen that the crust partly covered the heater grid in the lower part of the test section. Thus, part of the generated heat was dissipated in the crust.



Figure 15: Post test view of crust in LIVE-L1.

The calculated crust thickness at the end of the experiment is compared with the experimental profile in Figure 16. For the heat conductivity of the crust, a constant value of 0.45 W/(m K) was applied. Taking not into account power dissipation inside the crust, the crust thickness at in the lower part of the vessel is strongly over-estimated. Thus, heating of the crust has been considered in the lower third (up to 10 cm) of the pool. Since it is difficult to exactly assess the power released inside the crust, it has been assumed that the volumetric power in the crust is a fraction of the volumetric power in the pool. Taking a fraction of 30%, good agreement with the experimental crust thickness profile was reached, see curve labelled with “Model” in Figure 16.

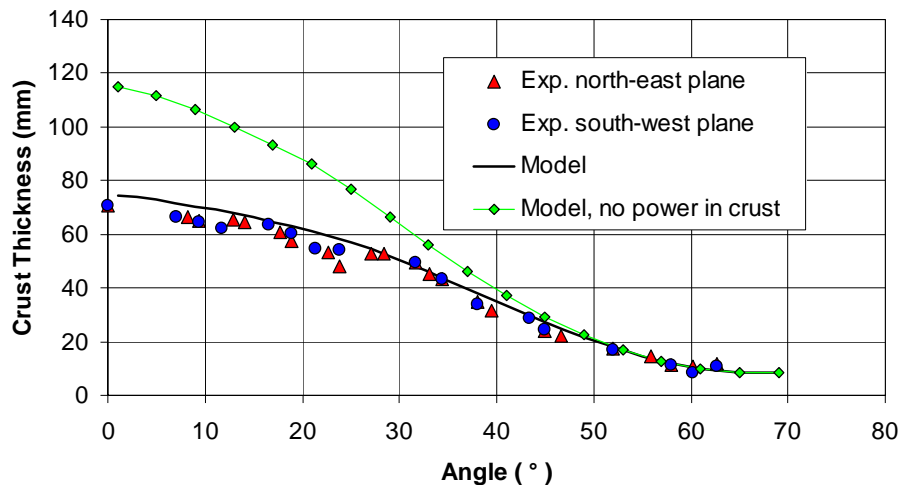
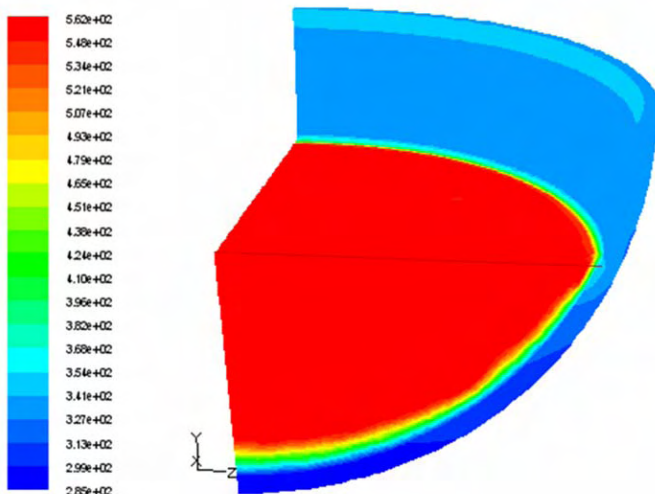


Figure 16. Calculated and measured crust thickness profile at the end of the test

### D.3 APPLICATION OF PECM SIMULATION MODEL

The Effective Convectivity Model (ECM) originates from the concept of the Effective Convectivity Conductivity Model (ECCM), but uses only the effective convectivity model and follows a different concept for the implementation. Recently, the method was extended for Phase-change problems to the so called PECM. In the PECM, a single transient enthalpy conservation equation is solved, which is common for solid and liquid regions. It considers conduction, convection, volumetric heat source and latent heat from phase change. If the temperature is between solidus and liquidus temperature, local thermal equilibrium between melt and solid is assumed (existence of a mushy zone).

In order to model the convective heat transport with the PECM method, the velocity field for the melt has to be determined. As a major simplification, the PECM method uses directional characteristic velocities,  $U_{up}$ ,  $U_{down}$  and  $U_{side}$  instead of solving the mass and momentum conservation equations for the fluid velocity  $u$ , which would require a much larger computational effort. The characteristic velocities are defined such that



**Figure 17. Temperature distribution in the pool (final state) calculated with the PECM method.**

the convective (+ conductive) fluxes in the respective direction equal the heat flux over the respective cooled boundaries. Classical heat transfer correlations are used to calculate the boundaries heat fluxes, the Steinberner-Reineke correlations for the down and up-ward fluxes and the Chawla and Chan correlation for the sideways heat transfer [24]. In phase change problems, the presence of a two-phase region (mushy zone) is taken into account by decreasing the characteristic velocities with increasing solid volume fraction.

The PECM aims at enabling sufficiently accurate and detailed analysis of heat transfer in a complex, 3D geometry in a computationally effective manner (compared to CFD simulations) and should also be convenient for generating grids in complex geometry computational domains. Therefore, it was implemented in the commercial CFD code Fluent through User

Defined Function (UDF). A detailed description of the ECM and PECM method is presented in [24].

The PECM method was applied in validation calculations to the LIVE L-1 experiment. The simulation is performed in 3D geometry, modelling one fourth of the plenum a mesh as shown in Figure 17 using an unstructured, not very fine mesh. The electrical heating power of the experiment is implemented in the PECM as a heat source, varying with the molten pool volume which is changed during the experiment. The PECM calculates the liquid volume after each time step in order to extract the heat, artificially added to the domain (as described in [23] and [24]). Based on the value of liquid volume, the decay heat is re-calculated as a ratio of power to the current liquid volume. So the PECM is then capable to represent the realistic heat source like the electrical heating of the experiment, i.e. the internal heat is not applied to solid volumes. Where the crust is formed, the heat source is no more available.

The boundary conditions applied to the PECM simulation are as follows. The outer wall of the vessel is applied to convection heat transfer. The top melt surface was applied to radiation heat transfer. The upper part of the vessel inner surface, where the vessel contacts with air (not with the melt) is also applied to radiation heat transfer. The simulation is started with a plenum filled by hot liquid melt, the initial temperature is 330 °C (according to the beginning temperature of thermocouples). In the first two hours, the vessel wall is cooled by the air, afterward it is cooled by a water flow.

A temperature contour is shown in Figure 17. The PECM temperature evolutions are presented in Figure 18. Temperature evolution figures indicate that the PECM well predicts the complicated behaviour of vessel wall temperatures in a long time period (many tens hours). Predicted temperatures levels are fairly agreed with the experimental data. However, the maximum recorded temperature of the vessel wall predicted by the PECM is slightly lower than the experimental. This may relate to the more flat temperature profile of the PECM simulation compared with the realistic experimental temperature profile. The temperature profile of the experiment is more stratified, due to lack of a top cooling surface. This behaviour is not fairly reflected in the PECM. The difference of temperature behaviour in IT/OT 15 during the last hours (Figure 18) may due to the incorrect boundary condition applied to the vessel wall in the top region.

The heat fluxes of the last steady states are shown in Figure 19 (about 15 hours and 27 hours). The heat flux profile obtained by the PECM simulation agrees well with the heat flux measured at IT/OT 1, 3, 5 and 15 positions. In position IT/OT 11, the PECM predicted heat fluxes are higher than the experimental. This deviation can be explained by the peak value of the boundary layer correlation implemented in the PECM [23, 24].

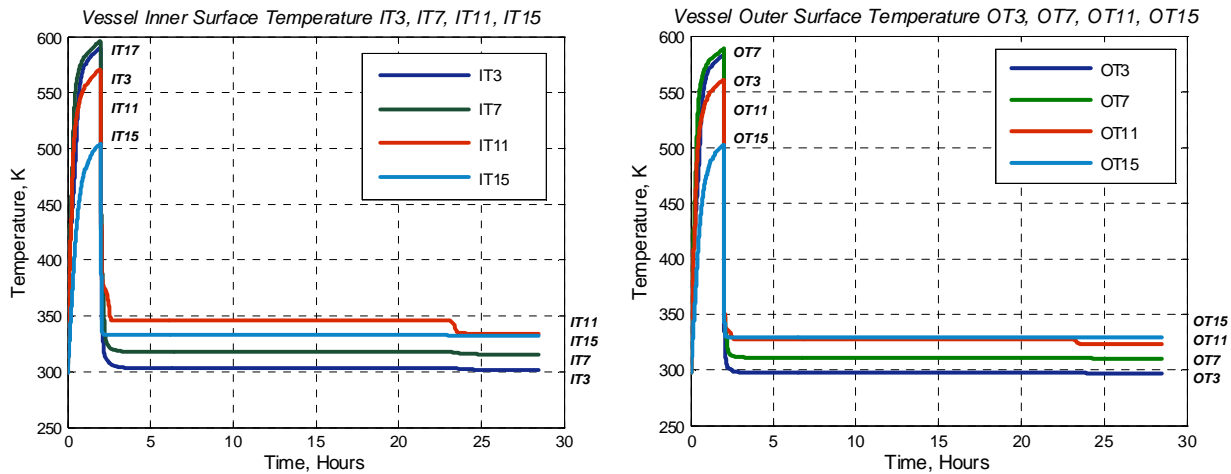


Figure 18. PECM temperature evolution of the vessel wall inner surface ( $IT_i$ ) and vessel wall outer surface ( $OT_i$ ). For comparison with experimental measurements cf. Figure 9 and Figure 10.

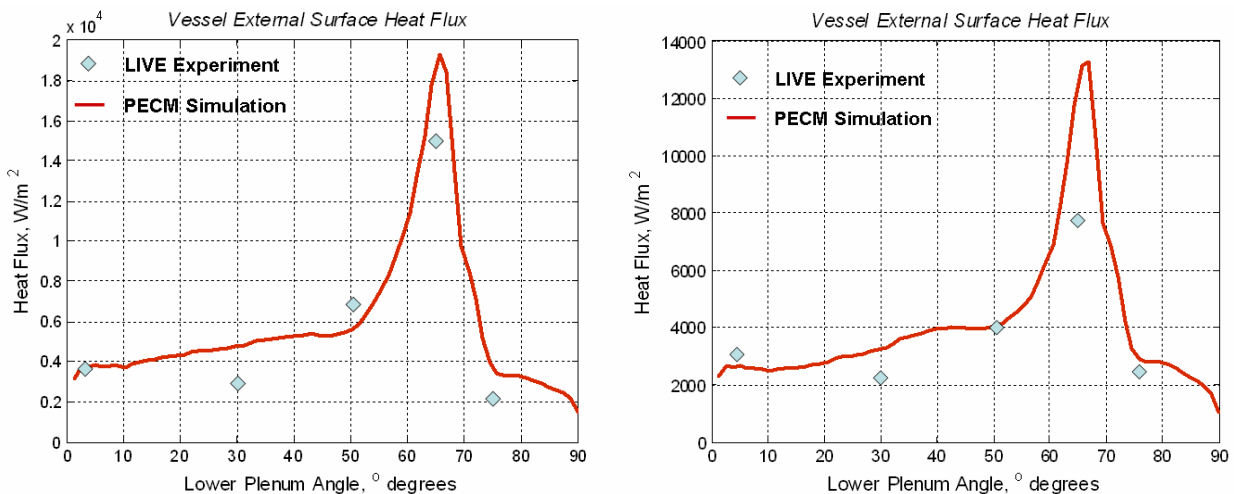


Figure 19. Outer vessel heat flux during steady state at 15 hours (left) and 27 hours (right).

Figure 20 shows the crust thickness predicted by the PECM and the experimental crust thickness (the dot line). As it is shown, the PECM result is reasonably well agreed with the experiment. The crust thickness of the PECM simulation in the lower region is thinner compared with the experimental (58.97 mm vs. 70.67 mm in the lowermost region). A larger experimental crust thickness of the lower region may be explained by two other probable reasons: more cold liquid is accumulated in this region from all the upper inclined surfaces of the crust, or the effect of non-uniform heated volume of the experiment (electrically heated) compared with the uniformly heated volume of the PECM simulation that causes an accumulation of cold liquid to be solidified in this region. The possible effect of accumulation of cold liquid in the lower region is difficult to be reflected in a simplified model. In addition, the other potential reason leading to the crust thickness difference is the different heating power distribution to the six layers of the melt pool. In the upper region of the melt pool, due to a high peaked heat flux of the boundary layer model implemented in the PECM, crust is not formed (see Figure 20).

The results of simulations show that the ECM and PECM are suitable tools for simulations of melt pool heat transfer.

#### D.4 APPLICATION OF THE CONV CODE TO THE SIMULATION OF THE FST4 LIVE TEST

CONV is a 3-D thermal-hydraulic CFD code [25, 26] for the simulation of heat transfer due to conduction and convection in complex geometry, crust formation, etc. It was developed at IBRAE (Nuclear Safety Institute of Russian Academy of Sciences, Moscow) within the framework of the International

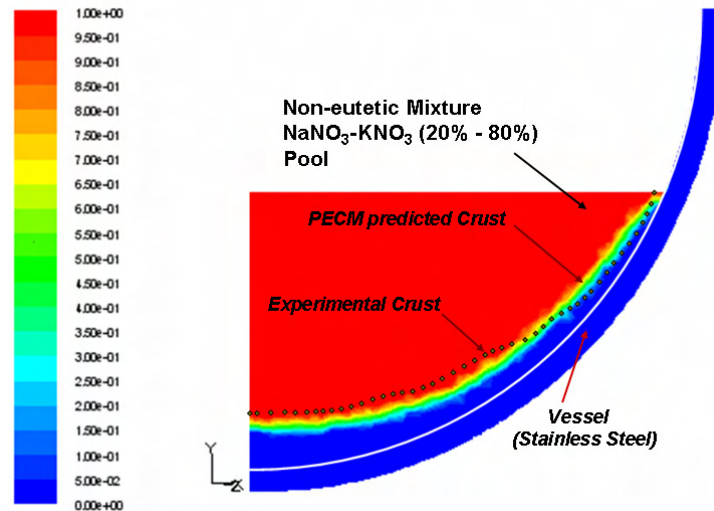


Figure 20. LIVE-L1 experiment and PECM predicted crust thickness.

RASPLAV project [27] to validate the concept of melt confinement in the reactor pressure vessel. Thereupon it was further improved within the ISTC 2936 Project and validated on numerous thermal-hydraulic tests.

For the modelling of a heat generating viscous liquid in a gravity field with consideration of the buoyancy force in a Boussinesq approximation, the efficient difference scheme [25, 26] is applied to solve the unsteady 3D Navier-Stokes equations in natural "velocity-pressure" variables on fully staggered orthogonal grids for Cartesian coordinates.

The CONV code was applied for the modelling of the LIVE FSt4 test. The FSt4 test was performed with water as working liquid. During the first 17930 s of the test the total heating power of app. 10 kW was applied to the pool. After reaching steady-state conditions, the power was completely switched off to observe the pool behaviour and temperature distribution in the liquid during the cool-down phase. The temperature was continuously measured during the test at several locations inside the pool.

An orthogonal curvi-linear grid with a nodalisation of  $201 \times 201$  meshes was used in the calculations. The grid was refined near the liquid/solid boundary and near the upper surface of the liquid (see Figure 21). The calculated temperature distribution during the steady-state phase of the test is presented in Figure 22. The comparison of the measured and calculated temperature evolution at two locations in the bulk of the liquid is given in Figure 25. The calculations correctly describe the heat-up and cool-down phases with minor overestimation of the temperature values during the steady-state phase of the test. In Figure 23 the

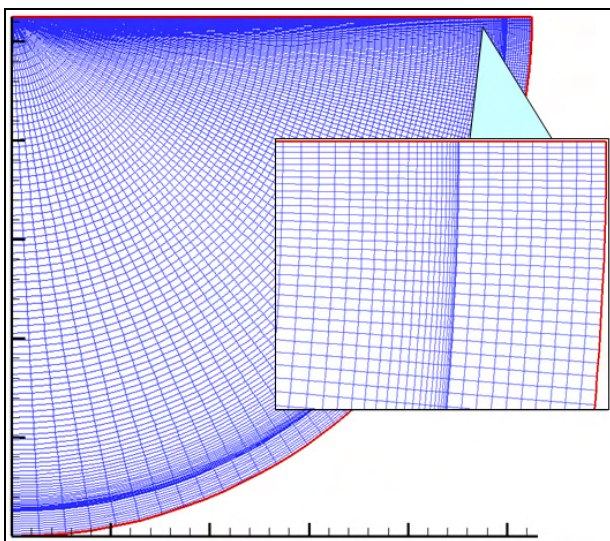


Figure 21. Type of nodalization scheme used in the calculations with CONV.

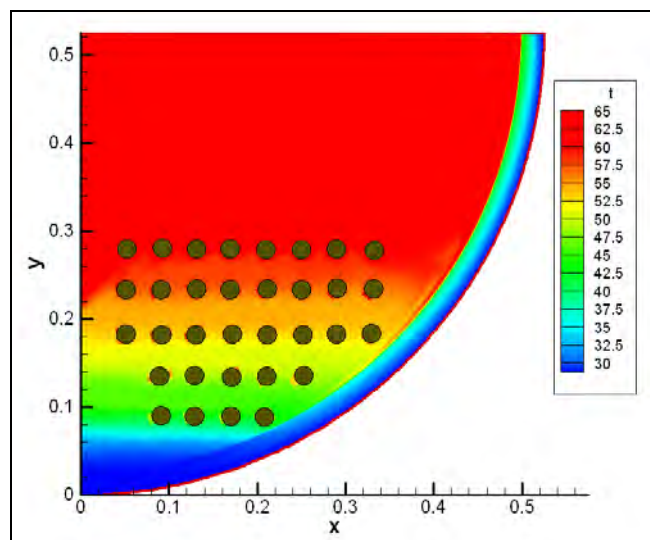


Figure 22. Temperature distribution calculated with CONV at the steady-state phase of the test. Symbols indicate thermocouple locations.

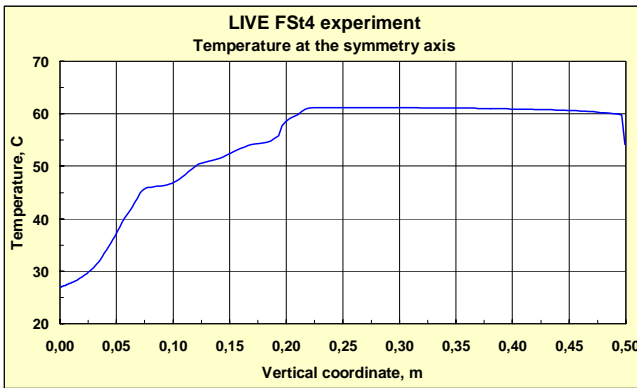


Figure 23 Temperature distribution along the symmetry axis of the pool calculated with CONV.

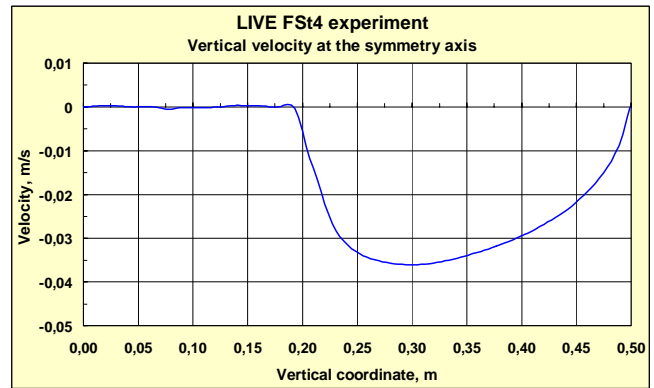


Figure 24. Vertical velocity distribution along the symmetry axis of the pool calculated with CONV.

temperature distribution along the vertical symmetry axis of the facility is presented. Liquid stratification with respect to temperature in the lower part of the pool (somewhat irregular due to specific location of the heaters) can be clearly observed, whereas the temperature in the upper part of the pool is almost uniform (i.e. the liquid is well-mixed due to intensive convection). This can be also seen in Figure 22.

The calculated vertical velocity distribution along the symmetry axis of the pool is presented in Figure 24. It is characterised by a stagnant zone in the lower part of the pool and sharp increase of the vertical velocity in the upper part, which is in agreement with the axial temperature distribution from Figure 23.

The comparison of the measured and calculated heat flux to the vessel wall at four locations during the steady state phase of the test is given in Figure 26. The first calculation assumes homogeneous heat generation in the liquid pool, the second one models the spiral heaters actually used in the test. The results show that there is no critical difference in the heat flux distribution at the vessel wall for these two cases, indicating that the LIVE facility adequately represents thermal conditions of the homogeneously heated liquid.

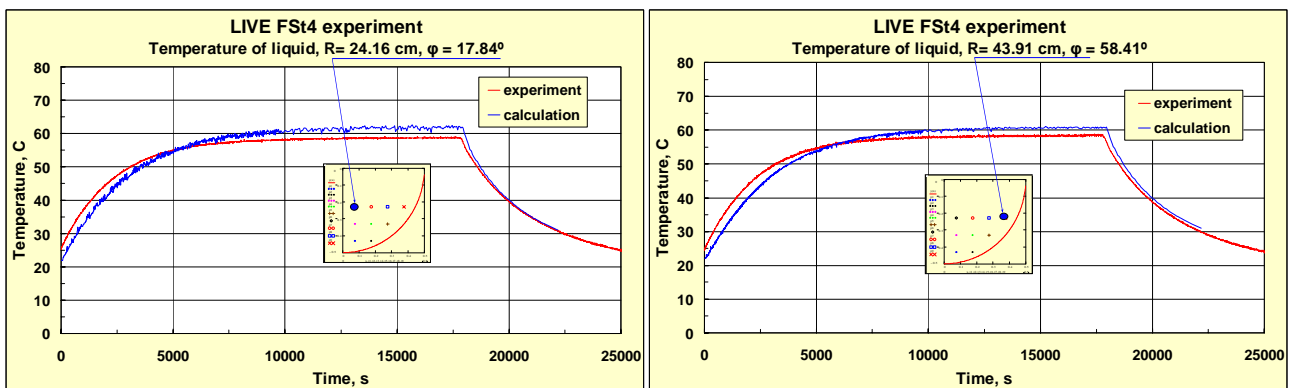


Figure 25. Measured and calculated temperature evolution at different locations in the bulk of liquid

## E CONCLUSIONS

The large-scale tests performed at FZK through the LIVE program complement the experimental data on melt pool behaviour. The tests are designed to support the analysis of core melt behaviour in the lower plenum of the reactor pressure vessel and the influence of the cooling of the vessel outer surface with water in the conditions that may occur during core meltdown accident in PWRs. In the test LIVE-L1 a binary non-eutectic mixture of  $\text{NaNO}_3$  and  $\text{KNO}_3$  was used to simulate the corium melt. To study the vessel thermal loadings during the melt relocation, the simulant melt was centrally poured into the LIVE hemispherical test vessel. The experimental protocol involved homogeneous volumetric heating of the melt during cooling of the outer RPV surface with air followed by the flooding of the vessel with water. The information obtained

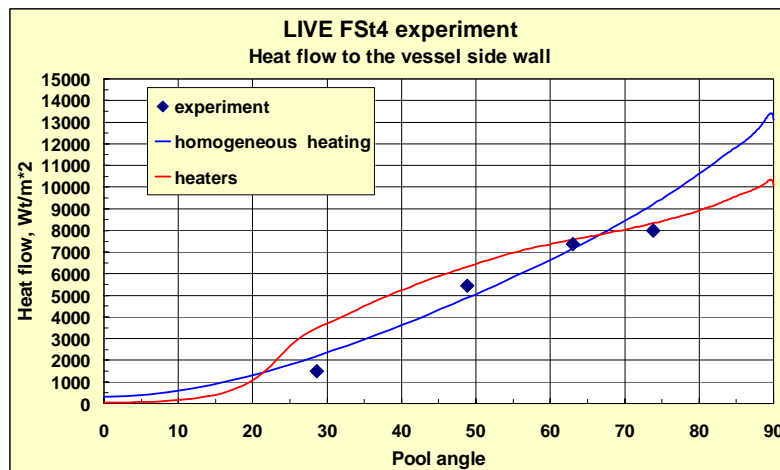


Figure 26. Measured and calculated heat flow to the side wall of the vessel.

from the LIVE-L1 experiment includes the melt temperature evolution during different stages of the test, the heat flux distribution along the reactor pressure vessel wall in transient and steady state conditions. In the post-test analysis, the crust thickness profile along the vessel wall, the crust composition and morphology were determined.

Experimental results of LIVE test were used for validation calculations applying models with different degree of detail. The stand-alone DIVA module (in-vessel core degradation and thermal hydraulics during a severe accident) of the ASTEC V1.3 code was applied by CEA to the analysis of the test LIVE-L1. For the ASTEC code a major requirement is fast execution time, therefore a lumped parameter approach is applied for the modelling of molten pools, based on empirical correlations for heat transfer. In the analysis, the molten pool was treated as a single layer. With the given simplifications, the results were fair. The calculated melt temperature was globally 10 to 20 K lower than the measured temperatures. For the inner and outer vessel wall temperatures, DIVA computed a too flat temperature profile compared to the experimental measurements. The calculation matched the maximum temperature and heat flux at the upper edge of the pool, but overestimated temperatures at lower locations by at most 40 K. The crust thickness at the end of the experiment was calculated using the simplified approach assuming steady-state conditions and linear temperature gradient through the crust. The results were in good agreement with the experimental values when a crust thermal conductivity slightly above the experimental estimates was used.

For the modelling of the vessel external cooling with water in natural convection can be performed with the CESAR module of the ASTEC code. This would eliminate uncertainties related to the imposed boundary conditions used in the present calculation. Some preliminary results of the DIVA-CESAR application being encouraging; they will be pursued in the near future. The simulation of the natural convection flow is very important for the analysis of in-vessel retention as a SAM strategy. Moreover, these calculations should be compared to the results from other codes (e.g. peer to peer RELAP calculations).

The molten pool model implemented in the late phase modules developed by IKE for the German system code ATHLET-CD also applies a simplified approach. It is based on a representative model of the pool, which takes into account an axial temperature profile in the pool. The sideways heat transfer is modelled using a boundary layer approach. For heat transfer to crusts, a sharp interface is assumed, implying liquidus temperature corresponding to melt composition as boundary condition. The calculations performed for the LIVE-L1 experiment showed quite good agreement with the measured melt and vessel wall temperatures and also reproduced the relatively steep axial heat flux profile, if the heat flux to the top of the pool was reduced. In variation calculations, the application of empirical correlations derived from the BALI and ACOPO experiments to the LIVE-L1 test was checked. The resulting heat flux distributions were too flat compared to the measurements, which can be explained by the low cooling rates at the top of the pool (exposed to air) in the present LIVE test. From the calculations with the MEWA/VECO pool model it was further concluded, that heat release inside the crust has to be considered for the lower part of the pool, where the crust partially covers the heating grid. Otherwise, the predicted crust thickness is too large.

A three-dimensional analysis with higher spatial resolution of the temperature field in the molten pool also for the LIVE-L1 test was carried out with the PECM method being developed by KTH, which is implemented in the CFD code Fluent. The time development of temperatures and calculated heat fluxes during the steady states agreed well with the measurements, with some over-prediction at the upper edge of the pool. This deviation was explained by the peak value of the boundary layer correlation implemented in the PECM. Also the crust profile predicted by the PECM method is close to the measured crust thickness.

The results of the PECM simulation are based on the concept of a mushy region at the pool/crust boundary, while the modelling in DIVA and MEWA assumes a sharp interface. In future analyses, more detailed comparisons between these competing approaches as well as with experimental results should be done in order to support the convergence towards a common, accepted modelling.

The calculations for the LIVE-L1 experiment with salt melt in the present paper were further complemented by analyses of the LIVE FSt4 test using water as melt simulant. They were carried out with the CONV CFD code, which was developed at IBRAE (Nuclear Safety Institute of Russian Academy) in the frame of RASPLAV and ISTC Projects and which is currently also applied for analysis of LIVE test at FZK. The presented for the LIVE FSt4 test showed that the experiment results can be quite accurately predicted by the CFD simulation. It is therefore expected that future analyses with of the CONV code also applied to other LIVE tests will provide valuable support for understanding and improvement of model in severe accident codes.

## REFERENCES

1. O. Kymäläinen et al., “In-Vessel Retention of Corium at the Loviisa Plant”, *Nucl. Eng. Design*, **169**, pp. 109-130 (1997).
2. S. Alabin et al., “The Results and Analysis of the RASPLAV Salt Tests“, *Proc. of the RASPLAV Seminar*, Munich, Germany, 14-15 November (2000).
3. T. G. Theofanous and S. Angelini, “Natural Convection for In-Vessel Retention at Prototypic Rayleigh Numbers”, *Nucl. Eng. Design*, **200**, pp. 1-9, (2001).
4. V. Asmolov et al., “Challenges Left In the Area of In-Vessel Melt Retention, *Nucl. Eng. Design*, **209**, pp. 87-96 (2001).
5. M. Helle et al. ““Experimental Data on Heat Flux Distribution from a Volumetrically Heated Pool with Frozen Boundaries”, Proceedings of In-Vessel Core Debris Retention and Coolability Workshop, Garching, Germany, March 3-6, pp. 173-183, 1998.
6. L. Bernaz et al. “Thermal Hydraulic Phenomena in Corium Pools: Numerical Simulation with TOLBIAC and Experimental Validation with BALF”, Proceedings of In-Vessel Core Debris Retention and Coolability Workshop, Garching, Germany, March 3-6, pp. 185-193, 1998.
7. B. Fluhrer et al., “The Experimental Programme LIVE to Investigate In-Vessel Core Melt Behaviour in the Late Phase”, *Proc. of the Jahrestagung Kerntechnik 2005*, INFORUM GmbH, Nürnberg, Germany, pp. 198-201 (2005).
8. A. Miassoedov et al., “Results of the LIVE-L1 Experiment On Melt Behaviour in RPV Lower Head Performed Within the LACOMERA Project at the Forschungszentrum Karlsruhe”, *Proc. of the 15th Internat. Conf. on Nuclear Engineering (ICONE-15)*, Nagoya, Japan (2007).
9. T. Albiol et al., “Overview of SARNET Deployment and Progress”, *Proc. of the ERMSAR-2007*, Karlsruhe, Germany, June 12-14 (2007).
10. J. P. Van Dorsselaere et al., “Overview of Progress of ASTEC Topic”, *Proc. of the ERMSAR-2007*, Karlsruhe, Germany, June 12-14 (2007).
11. E. M. Levin, *Phase Diagrams For Ceramists Vol. 1: Oxides and Salts*, American Ceramic Society, ISBN-10: 0916094049 (1986).

12. A. Miassoedov et al., “Large Scale Experiments on Core Degradation, Melt Retention and Coolability (LACOMERA)”, *Proc. of the FISA-2003. EU Research in Reactor Safety*, Luxembourg, November 10-13 (2003).
13. L. Godin-Jacqmin, A. Bachrata, “Analysis of the LIVE-L1 experiment with the ASTEC V1.3 code”, SARNET /ASTEC report, CEA/DEN/DTN/STRY/LMA/2007-031 (2007).
14. B. Sehgal et al., “Ex-vessel Core Melt Stabilization Research,” Report SAM-ECOSTAR-D26 (2002).
15. G. Guillard et al., “ASTEC V1 code : DIVA physical modelling,” *ASTEC-VI/DOC/06-17* (2006).
16. A. Miassoedov et al., “Application of the ASTEC V1 Code to the LIVE-L1 Experiment”, *Proc. of ICAPP '08*, Anaheim, USA, June 8-12 (2008).
17. D. Tarabelli et al., “ASTEC Application to In-Vessel Corium Retention,” *Proc. of the ERMSAR-2007*, Karlsruhe, Germany, June 12-14 (2007).
18. K. Trambauer, C. Bals, J.-D. Schubert and H. Austregesilo, “ATHLET-CD Mod 2.1 - Cycle A User’s Manual”, Gesellschaft für Anlagen- und Reaktorsicherheit (GRS), *GRS-P-4/Vol. 1*, July 2006.
19. J. M. Bonnet, “An integral model for the calculation of heat flux distribution in a pool with internal heat generation”, *Proceedings NURETH-7*, Saratoga, USA (1995).
20. T. W. Chawla and S. H. Chan “Heat transfer for vertical/inclined boundaries of heat generating boiling pools”, *J. Heat Transfer*, Vol. 104, pp. 465 (1982).
21. M. Buck, “Modelling of the Late Phase of Core Degradation in Light Water Reactors”, Dissertation, Universitaet Stuttgart, *IKE 2-153*, November 2007.
22. J.M. Seiler et al., “Experimental Results obtained in France in Support of In Vessel Retention”, *Proceedings of RASPLAV seminar 2000*, Munich, November 14-15 (2000).
23. C. T. Tran, T. N. Dinh, “An Effective Convectivity Model for Simulation of In- Vessel Core Melt Progression in Boiling Water Reactor”, 2007 International Congress on Advances in Nuclear Power Plants (ICAPP 2007), Nice Acropolis, France, May 13-18, (2007).
24. C. T. Tran and T. N. Dinh, “Simulation of Core Melt Pool Formation in a Reactor Pressure Vessel Lower Head Using an Effective Convectivity Model”, *Proceedings, International Topical Meeting on Nuclear Reactor Thermal Hydraulics – NURETH-12*, Pittsburgh, Pennsylvania, USA, September 30 – October 04 (2007).
25. A.E.Aksenova, V.V.Chudanov, V.A.Pervichko, V.N.Semenov, V.F.Strizhov “Development and application of the CONV Codes”. *Proceedings of RASPLAV seminar 2000*, Munich, November 14-15 (2000).
26. A.Aksenova, V.Chudanov, A.Churbanov, V.Pervishko, A.Popkov, V.Strizhov, P.Vabishchevich, V.Varenkov, CONV2D: An Integrated Computer Code for Numerical Modelling of Convection/Diffusion Processes with regard for Melting. Nuclear Safety Institute (IBRAE), May 1997.
27. V.Asmolov, “RASPLAV Project: Major Activities and Results”, *Proceedings of RASPLAV seminar 2000*, Munich, Germany, November 14-15 (2000).